

A novel finite-volume TVD scheme to overcome non-realizability problem in quadrature-based moment methods

Original

A novel finite-volume TVD scheme to overcome non-realizability problem in quadrature-based moment methods / Shiea, Mohsen; Buffo, Antonio; Vanni, Marco; Marchisio, Daniele L.. - In: JOURNAL OF COMPUTATIONAL PHYSICS. - ISSN 0021-9991. - 409:(2020), p. 109337. [10.1016/j.jcp.2020.109337]

Availability:

This version is available at: 11583/2797743 since: 2020-02-26T11:17:15Z

Publisher:

Elsevier

Published

DOI:10.1016/j.jcp.2020.109337

Terms of use:

This article is made available under terms and conditions as specified in the corresponding bibliographic description in the repository

Publisher copyright

(Article begins on next page)

A novel finite-volume TVD scheme to overcome non-realizability problem in quadrature-based moment methods

Mohsen Shiea^a, Antonio Buffo^{a,*}, Marco Vanni^a, Daniele L. Marchisio^a

^a*Dipartimento di Scienza Applicata e Tecnologia, Politecnico di Torino, Corso Duca degli Abruzzi 24, 10129 Torino, Italy*

Abstract

A new finite-volume total variation diminishing (TVD) scheme is proposed for the solution of moment transport equations in quadrature-based moment methods (QBMM). The proposed scheme is capable of preserving important properties of the moments, such as realizability and boundedness. The idea behind the approach is to limit the flux of all the moments at each cell face with the same limiter value. The proposed numerical technique was eventually compared with other realizable schemes developed for the moment transport equations, showing that the method is able to keep the moments realizable and bounded at the same time.

Keywords: Quadrature-based moment methods (QBMM); Moment realizability; Moment boundedness; Population balance equation (PBE); High-resolution scheme; Finite-volume method.

1. Introduction

The evolution in space and time of a population of disperse elements (e.g., droplets, bubbles or particles moving in a continuous fluid) can be described by using an Eulerian approach through the solution of a generalized

*Corresponding author; current mailing address: Dipartimento di Scienza Applicata e Tecnologia, Politecnico di Torino, Corso Duca degli Abruzzi 24, 10129 Torino, Italy; email: antonio.buffo@polito.it; tel.: +390110904758.

5 population balance equation (GPBE). It is an integro-differential equation
6 written in terms of a number density function (NDF) representing, at every
7 point of the physical space, the number of elements that have a particular
8 state belonging to the so-called phase space, i.e. the space of the properties
9 required to characterize the system under investigation (e.g. element size, ve-
10 locity, chemical composition, temperature). The Quadrature-Based Moment
11 Methods (QBMM) are proved to be efficient in solving the GPBE, where the
12 transport equations for some moments of the underlying NDF are solved in-
13 stead of the GPBE [1]. These methods are based on the assumption that the
14 underlying NDF has the form of a multi-dimensional summation of weighted
15 kernel density functions (KDF) centered on the quadrature abscissas, where
16 the quadrature weights and abscissas can be retrieved from the moments by
17 means of the so-called inversion algorithms (such as the Product-Difference
18 (PD) [2] and the Chebyshev [3] algorithms). In most cases, the KDF is a
19 Dirac delta function, especially when a continuous reconstruction of the NDF
20 is not necessary. While these methods are efficient and promising, especially
21 when coupled with Computational Fluid Dynamics (CFD) codes, their prac-
22 tical use encounters inherent difficulties to cope with. One major issue is
23 the realizability or consistency of the transported moment set, meaning that
24 there must exist an underlying number density function (NDF) corresponding
25 to the transported moments. Confining the discussion to the finite-volume
26 method, the most common cause of the non-realizability (also known as nu-
27 merical moment corruption) lies in the spatial discretization of the transport
28 term of the moment equation, when high-order spatial discretization schemes
29 are used. This problem is often related to the convective term, as in many

30 cases the governing equations have a hyperbolic form. Desjardins et al. [4]
31 demonstrated that the 1st-order scheme guarantees the realizability of the
32 moments, provided the CFL condition is respected. However, this scheme
33 results in highly diffusive solutions, leading sometimes to unacceptable pre-
34 dictions, hence the necessity of adopting high-order schemes. On the other
35 hand, employing high-order finite-volume schemes for independent transport
36 of the moments may cause non-realizability issues [5]. Therefore, the devel-
37 opment of a realizable high-order scheme for the solution of moment trans-
38 port equations is crucial. In this regard, Vikas and co-workers [6] presented
39 the so-called realizable quasi-high-order schemes, based on the evaluation
40 of the moment fluxes at the cell faces using the interpolated abscissas and
41 weights of the quadrature. With this method, the quadrature interpola-
42 tion is performed by applying 1st-order scheme to the quadrature abscissas
43 and high-order schemes to the quadrature weights. This approach produces
44 less diffusive solutions and guarantees the realizability of the transported
45 moments, provided a criterion on the time step is respected. However, no
46 analysis was conducted on the boundedness property of this approach, which
47 can not be ignored since unbounded predictions are not physically allowed
48 [7]. Kah et al. [8] formulated a 2nd-order kinetic scheme that makes use of
49 the canonical moments to transport the moments indirectly while maintain-
50 ing them in the moment space. However, the application of their method
51 to simulations with more than four moments involves difficult algebra [9].
52 Recently, Laurent and co-workers [9] developed a similar approach based on
53 reconstructing the coefficients ζ_k (for its definition refer to [9]) instead of the
54 canonical moments. However, their original ζ_k reconstruction based scheme

55 cannot be applied easily to the unstructured grids and therefore they sug-
56 gested a simplified version of this scheme that involves division of the cells
57 into three parts as proposed by Berthon [10].

58 The present work introduces a new technique, called equal-limiter scheme,
59 to overcome the non-realizability problem when 2nd-order TVD (Total Vari-
60 ation Diminishing) schemes are applied to the moment transport equations.
61 The technique is based on using an equal limiter given by the flux-limiter
62 function for all the moments, and it will be shown that it is effective to
63 avoid non-realizable set of moments. Moreover, its application to three-
64 dimensional unstructured grids is straightforward. The paper is organized as
65 follows. First, it will be proved that, in a one-dimensional Riemann problem,
66 the concept of equal-limiter emerges naturally if no source term is included in
67 the moment transport equations. Next, the importance of using an identical
68 limiter given by the limiter function for all the moments will be clarified in
69 a general case by solving local Riemann problem at each cell face and the
70 role of the time step in maintaining the realizability of the moments will be
71 explained. Moreover, the paper shows how this technique can be applied to
72 CFD codes, without any assumption on velocity field or type of mesh grid. In
73 the final part, a comparison between different techniques will be performed
74 by solving moment transport equations in some one- and two-dimensional
75 test cases.

76 2. TVD scheme for moment transport equation

77 2.1. Moment transport equation

78 As previously mentioned, QBMM deal with the solution of the trans-
79 port equations written in terms of the moments of the NDF, instead of the
80 GPBE itself. The NDF is a complex multi-dimensional functional that de-
81 pends on the so-called external coordinates, i.e. the position of the elements
82 in the physical space and time, and on the internal coordinates, which are
83 the generic properties associated to each element of the population, such as
84 size, velocity, chemical composition or temperature. When the internal co-
85 ordinates do not include the velocity of the elements of the disperse phase,
86 the resulting transport equation for the NDF is called Population Balance
87 Equation (PBE) [1]. Although it is possible to apply the proposed numerical
88 scheme to the transport equation for a multivariate set of moments, let us
89 consider a univariate PBE with the size of the elements of the disperse phase,
90 L , as the internal coordinate, for the sake of simplicity and clarity. In this
91 case, the PBE can be written as follows [11]:

$$\frac{\partial f}{\partial t} + \frac{\partial(\mathbf{U}f)}{\partial \mathbf{x}} + \frac{\partial(\dot{L}f)}{\partial L} = h \quad (1)$$

92 where $f \equiv f(L, \mathbf{x}, t)$ denotes the NDF. In addition, $\mathbf{U} \equiv \mathbf{U}(\mathbf{x}, t)$ is the
93 velocity of the disperse phase, \dot{L} represents the continuous rate of change
94 in the size of elements due to the continuous processes (e.g. mass transfer
95 driven growth) and h introduces the contribution of the discrete events (e.g.
96 aggregation/breakage) into the PBE. It is worth remarking that the velocity
97 of the disperse phase appearing in Eq. (1) does not depend on the size of

98 the elements: such approximation has been made to simplify the following
 99 discussion and it is not a limitation of the proposed approach.

100 By definition, the k^{th} -order moment of f with respect to L is:

$$M^k(\mathbf{x}, t) = \int_0^\infty f(L, \mathbf{x}, t) L^k dL \quad (2)$$

101 The importance of the moments lies in the fact that lower-order moments
 102 are associated to various integral properties of the population. For instance,
 103 in this case the 3rd-order moment with respect to L is proportional to the
 104 volume fraction of the disperse phase. The above definition can be used to
 105 derive moment transport equations from Eq. (1). For the sake of simplicity,
 106 from now on we assume a one-dimensional case where the velocity is constant
 107 (u) and the contribution of the continuous processes is negligible ($\dot{L} = 0$).
 108 The transport equation for the k^{th} -order moment reduces to the following
 109 partial differential equation:

$$\frac{\partial M^k}{\partial t} + u \frac{\partial M^k}{\partial x} = \bar{h}^k \quad (3)$$

110 where \bar{h}^k is the source term changing the k^{th} -order moment due to the discrete
 111 events. Generally, this source term is a complex multi-dimensional integral
 112 which depends on the NDF itself. QBMM employ the so-called quadrature
 113 approximation to express the functional form of the NDF. If we consider
 114 only one internal coordinate, it is possible to write a generic integral in the
 115 following way and therefore close the moment transport equations:

$$\int_{\Omega_L} f(L)g(L)dL = \sum_{\alpha=1}^N w_\alpha g(L_\alpha) \quad (4)$$

116 where w_α and L_α are the weights and abscissas of the N -node quadrature
 117 formula. This means that the NDF is approximated as a summation of delta

118 functions centered on quadrature abscissas:

$$f(L) = \sum_{\alpha=1}^N w_{\alpha} \delta(L - L_{\alpha}) \quad (5)$$

119 This method is called Quadrature Method of Moments (QMOM) and it is
120 designed to solve univariate PBE [12]. The weights and abscissas are deter-
121 mined from the transported moments by employing an inversion algorithm
122 (such as PD or Chebyshev algorithms), provided the set of moments is re-
123 alizable. This is usually referred as the moment problem [13]: in particular,
124 when the support of the NDF is $\Omega_L =]0, +\infty[$ as in this case, it is called
125 finite Stieltjes moment problem. When the support of the NDF is different,
126 i.e. $\Omega_L =]-\infty, +\infty[$ or $\Omega_L =]0, 1[$, we refer to finite Hamburger and finite
127 Hausdorff moment problems respectively. These three different supports re-
128 sult in different constraints on the transported set of moments to ensure
129 its realizability [13, 14]. However, the non-realizability problem is common
130 to all these cases and poses the main challenge in practical applications of
131 QMOM. In the finite-volume method, this can happen particularly during
132 the interpolation of the moments on to the faces to calculate the flux of the
133 moments through faces if high-resolution TVD schemes are employed.

134 2.2. Finite-Volume Method

135 As mentioned before, the present study focuses on the non-realizability
136 issue in the context of the finite-volume method. The general formulation
137 of the finite-volume method can be found in the specialized literature [15,
138 16], and therefore is omitted here. Let a single-stage explicit method be
139 adopted to march in time and the source terms be handled using fractional-
140 step approach [15]. In this way, the finite-volume method transforms Eq. (3)

141 into the following discretized form written for the generic cell i of size Δx in
 142 the spatial domain:

$$M_i^{k*} = M_i^k - \frac{\Delta t}{\Delta x} (F_{i+1/2}^k - F_{i-1/2}^k) \quad (6)$$

$$(M_i^k)^{n+1} = M_i^{k*} - \Delta t \bar{h}_i^k \quad (7)$$

143 where M_i^k , M_i^{k*} and $(M_i^k)^{n+1}$ refer to, respectively, the moment value at the
 144 current time (t_n), the intermediate value of the fractional-step approach and
 145 the moment value at the new time (t_{n+1}) after a time step of Δt . Further-
 146 more, $F_{i-1/2}^k$ and $F_{i+1/2}^k$ denote the numerical flux along the left and right
 147 faces of the cell i respectively, each depends on the neighboring cell values at
 148 time t_n according to the selected numerical flux function. From now on, the
 149 primary focus of the work will be on Eq. (6), particularly the calculation of
 150 the flux of the moments at the faces. The effect of the source term will be
 151 clarified afterwards.

152 It is desirable to calculate the fluxes using high-resolution schemes, which
 153 are on the basis of slope-limiter methods. These methods use a high-order
 154 scheme where the solution is smooth enough, otherwise they switch to a low-
 155 order one to prevent non-physical oscillations in the numerical solution [15].
 156 In this way, the solution exhibits higher order of accuracy, comparing to 1st-
 157 order solution, without losing the boundedness. Using Lax-Wendroff as the
 158 high-order scheme and upwind as the low-order one will form the so-called
 159 flux-limiter methods with the following numerical flux functions [15]:

$$F_{i-1/2}^k = u^- M_i^k + u^+ M_{i-1}^k + \frac{1}{2} |u| \left(1 - \frac{|u| \Delta t}{\Delta x} \right) \phi(\theta_{i-1/2}^k) \Delta M_{i-1/2}^k \quad (8)$$

$$F_{i+1/2}^k = u^- M_{i+1}^k + u^+ M_i^k + \frac{1}{2} |u| \left(1 - \frac{|u| \Delta t}{\Delta x} \right) \phi(\theta_{i+1/2}^k) \Delta M_{i+1/2}^k \quad (9)$$

160 where

$$u^+ = \frac{1}{2}(u + |u|) \quad \text{and} \quad u^- = \frac{1}{2}(u - |u|) \quad (10)$$

161 In addition, $\Delta M_{i-1/2}^k$ and $\Delta M_{i+1/2}^k$ are respectively the jumps across the left
162 and right faces, defined following the below convention:

$$\Delta M_{i-1/2}^k = M_i^k - M_{i-1}^k \quad (11)$$

163 The flux-limiter ϕ is a function of the smoothness of M^k at the face ($\theta_{i\pm 1/2}^k$).

164 The smoothness is commonly defined as follows [15]:

$$\theta_{i-1/2}^k = \frac{\Delta M_{I-1/2}^k}{\Delta M_{i-1/2}^k} \quad \text{with} \quad I = \begin{cases} i-1 & \text{if } u \geq 0 \\ i+1 & \text{if } u < 0 \end{cases} \quad (12)$$

165 A variety of flux-limiter functions are available in the literature such as min-
166 mod [17] and van Leer [18].

167 Substituting the numerical fluxes in Eq. (6) yields the following dis-
168 cretized equation:

$$M_i^{k*} = M_i^k - \frac{\Delta t}{\Delta x} u^+ (M_i^k - M_{i-1}^k) - \frac{\Delta t}{\Delta x} u^- (M_{i+1}^k - M_i^k) - \frac{1}{2} \frac{|u| \Delta t}{\Delta x} \left(1 - \frac{|u| \Delta t}{\Delta x} \right) \left[\phi(\theta_{i+1/2}^k) \Delta M_{i+1/2}^k - \phi(\theta_{i-1/2}^k) \Delta M_{i-1/2}^k \right] \quad (13)$$

169 3. The Concept of Equal-Limiter

170 The flux-limiter methods were developed to address the issue of bound-
171 edness that occurs in the case of employing high-order schemes to solve hy-
172 perbolic problems. One would ideally desire to use these methods for the
173 solution of the moment transport equations, particularly when the 1st-order

174 accuracy is not sufficient to describe the behavior of the system under study.
 175 However, in general, the non-realizability problem hinders their direct prac-
 176 tice in solving the moments transport equations. In this section, it is shown
 177 that this limitation can be overcome by selecting an equal limiter for all the
 178 moments.

179 The starting point is to show that the idea of equal-limiter emerges in
 180 the case of employing 2nd-order TVD schemes for the pure moment advection
 181 with no source term ($(M_i^k)^{n+1} = M_i^{k*}$) in a Riemann problem example. It
 182 will be also shown that in this case the moments remain realizable. Then, the
 183 discussion will continue to highlight the advantage of employing equal-limiter
 184 in a more general context, where the effect of aggregation and breakage will
 185 be also taken into account.

186 The argument begins with rewriting Eq. (13) for the case $u > 0$ without
 187 loss of generality¹:

$$(M_i^k)^{n+1} = M_i^k - \nu(M_i^k - M_{i-1}^k) - \frac{1}{2}\nu(1-\nu) [\phi(\theta_{i+1/2}^k)\Delta M_{i+1/2}^k - \phi(\theta_{i-1/2}^k)\Delta M_{i-1/2}^k] \quad (14)$$

188 where $\nu = u\Delta t/\Delta x$ is the Courant number. The smoothness at the left and
 189 right faces are written as follows Eq. (12):

$$\theta_{i-1/2}^k = \frac{M_{i-1}^k - M_{i-2}^k}{M_i^k - M_{i-1}^k} \quad \text{and} \quad \theta_{i+1/2}^k = \frac{M_i^k - M_{i-1}^k}{M_{i+1}^k - M_i^k} \quad (15)$$

190 Now let us consider a Riemann problem example with the following initial

¹The case $u < 0$ can be formulated similarly and leads to the same conclusions

191 data:

$$M^k(x, 0) = \overset{\circ}{M}^k = \begin{cases} \overset{\circ}{M}_l^k & \text{if } x < 0 \\ \overset{\circ}{M}_r^k & \text{if } x > 0 \end{cases} \quad (16)$$

192 where $\overset{\circ}{M}_l^k$ and $\overset{\circ}{M}_r^k$ are obtained from the initial left and right NDFs, $\overset{\circ}{f}_l$ and $\overset{\circ}{f}_r$,
 193 and consequently constitute two realizable sets of moments. It is postulated
 194 that the numerical solution of the k^{th} -order moment at any generic cell i and
 195 any time step t_n , including the zero time, can be expressed as:

$$M_i^k = \overset{\circ}{M}_r^k - a_i^n (\overset{\circ}{M}_r^k - \overset{\circ}{M}_l^k) \quad , \quad 0 \leq a_i^n \leq 1 \quad (17)$$

196 where a_i^n is a constant that changes with the cell index i and the time step
 197 but not due to the moment order or value. In other words, this constant is
 198 the same for all the moments of a given cell at each time step. It is worth
 199 mentioning that the initial data (Eq. (16)) corresponds to $a_i^0 = 1$ for $x_i < 0$
 200 and $a_i^0 = 0$ for $x_i > 0$. Next step is to substitute Eq. (17) in Eq. (14), which
 201 after simplifications yields the following:

$$\begin{aligned} (M_i^k)^{n+1} &= \overset{\circ}{M}_r^k - a_i^n (\overset{\circ}{M}_r^k - \overset{\circ}{M}_l^k) + \nu (a_i^n - a_{i-1}^n) (\overset{\circ}{M}_r^k - \overset{\circ}{M}_l^k) \\ &\quad + \frac{1}{2} \nu (1 - \nu) \left[\phi \left(\frac{a_i^n - a_{i-1}^n}{a_{i+1}^n - a_i^n} \right) (a_{i+1}^n - a_i^n) \right. \\ &\quad \left. - \phi \left(\frac{a_{i-1}^n - a_{i-2}^n}{a_i^n - a_{i-1}^n} \right) (a_i^n - a_{i-1}^n) \right] (\overset{\circ}{M}_r^k - \overset{\circ}{M}_l^k) \\ &= \overset{\circ}{M}_r^k - a_i^{n+1} (\overset{\circ}{M}_r^k - \overset{\circ}{M}_l^k) \end{aligned} \quad (18)$$

202 and a_i^{n+1} collects several coefficients that do not depend on the moment

203 values:

$$\begin{aligned}
a_i^{n+1} = & a_i^n - \nu(a_i^n - a_{i-1}^n) \\
& - \frac{1}{2}\nu(1 - \nu) \left[\phi \left(\frac{a_i^n - a_{i-1}^n}{a_{i+1}^n - a_i^n} \right) (a_{i+1}^n - a_i^n) \right. \\
& \left. - \phi \left(\frac{a_{i-1}^n - a_{i-2}^n}{a_i^n - a_{i-1}^n} \right) (a_i^n - a_{i-1}^n) \right]
\end{aligned} \tag{19}$$

204 Equation (19) has the same structure of Eq. (14), therefore, it appears that
205 a_i^n is the solution of an advection equation for the variable a obtained by the
206 2nd-order TVD finite-volume scheme. As a consequence, it is guaranteed that
207 a_i^{n+1} remains bounded to the values of the previous time step, i.e. between
208 0 and 1. Now it can be concluded that the postulated solution at time step
209 t_n is also valid at the next time step t_{n+1} :

$$(M_i^k)^{n+1} = \overset{\circ}{M}_r^k - a_i^{n+1}(\overset{\circ}{M}_r^k - \overset{\circ}{M}_i^k), \quad 0 \leq a_i^{n+1} \leq 1 \tag{20}$$

210 As mentioned before, the initial data (Eq. (16)) can be expressed by Eq. (17),
211 therefore, the postulated solution is indeed the solution of Eq. (14) at any
212 time step with the initial data defined by Eq. (16). Moreover, it can be
213 proved that the solution guarantees the realizability of the moments at any
214 time step if the initial set is realizable. To proceed with the proof, the
215 following notation is used for representing the set of moments:

$$\mathbf{W} = [M^0 \quad M^1 \quad \dots \quad M^{2N-1}]^T \tag{21}$$

216 It is worth reiterating that N is the number of quadrature nodes. The set of
217 moments can be defined as follows:

$$\mathbf{W} = \int_0^\infty f(L)\mathbf{q}(L)dL \tag{22}$$

218 where $\mathbf{q}(L) = [L^0 \ L^1 \ \dots \ L^{2N-1}]^T$.

219 Equation (20) can be written for the set of moments by using the notation
220 introduced in Eq. (21):

$$\mathbf{W}_i^{n+1} = \mathbf{W}_r - a_i^{n+1}(\mathbf{W}_r - \mathbf{W}_l) \quad (23)$$

221 It should be emphasized that Eq. (23) is derived based on the fact that a_i^{n+1}
222 is identical for all the moments. The proof follows by substituting Eq. (22)
223 in Eq. (23) and performing some manipulations:

$$\int_0^\infty f_i^{n+1} \mathbf{q}(L) dL = \int_0^\infty [(1 - a_i^{n+1}) \overset{\circ}{f}_r + a_i^{n+1} \overset{\circ}{f}_l] \mathbf{q}(L) dL \quad (24)$$

224 OR

$$f_i^{n+1} = (1 - a_i^{n+1}) \overset{\circ}{f}_r + a_i^{n+1} \overset{\circ}{f}_l \quad (25)$$

225 The above equation guarantees the non-negativity of the f_i^{n+1} because both
226 $\overset{\circ}{f}_r$ and $\overset{\circ}{f}_l$ are defined to be non-negative NDFs and $0 \leq a_i^{n+1} \leq 1$. Conse-
227 quently, the moment set of cell i at time step t_{n+1} is realizable, see [4].

228 Returning back to the equal-limiter concept, it was previously highlighted
229 that an identical a_i^{n+1} for all the moments is essential to keep the moment
230 set realizable in a Riemann problem example. The identical a_i^{n+1} originates,
231 in turn, from the equal limiters calculated at the left and right faces (i.e.,
232 Eq. (18)):

$$\phi(\theta_{i-1/2}^k) = \phi\left(\frac{a_{i-1}^n - a_{i-2}^n}{a_i^n - a_{i-1}^n}\right) \quad \text{and} \quad \phi(\theta_{i+1/2}^k) = \phi\left(\frac{a_i^n - a_{i-1}^n}{a_{i+1}^n - a_i^n}\right). \quad (26)$$

233 When source terms are present, the limiters are not generally identical for
234 all the moments, because in this case the smoothness of the moments may

235 change differently and this may cause the non-realizability of the transported
 236 moment set. This suggests to find a technique to employ an identical limiter
 237 in the calculation of the moment fluxes at the faces.

238 Again Eq. (13) is rewritten for the case of $u > 0$ (here a local Riemann
 239 problem is solved at each face of cell i):

$$M_i^{k*} = M_i^k - \nu(M_i^k - M_{i-1}^k) - \frac{1}{2}\nu(1-\nu)[\phi(\theta_{i+1/2}^k)\Delta M_{i+1/2}^k - \phi(\theta_{i-1/2}^k)\Delta M_{i-1/2}^k] \quad (27)$$

240 which can simply be expressed as follows by collecting the terms containing
 241 the moment of cells $i-1$, i and $i+1$:

$$M_i^{k*} = B_i^k M_{i-1}^k + C_i^k M_i^k - D_i^k M_{i+1}^k \quad (28)$$

242 with

$$\begin{aligned} B_i^k &= \nu - \frac{1}{2}\nu(1-\nu)\phi(\theta_{i-1/2}^k) \\ C_i^k &= 1 - \nu + \frac{1}{2}\nu(1-\nu)[\phi(\theta_{i+1/2}^k) + \phi(\theta_{i-1/2}^k)] \\ D_i^k &= \frac{1}{2}\nu(1-\nu)\phi(\theta_{i+1/2}^k) \end{aligned} \quad (29)$$

243 Writing Eq. (28) for the set of moments of order $k = 1, 2, \dots, 2N-1$ yields:

$$\begin{pmatrix} M_i^{0*} \\ M_i^{1*} \\ \vdots \\ M_i^{2N-1*} \end{pmatrix} = \underbrace{\begin{pmatrix} B_i^0 M_{i-1}^0 \\ B_i^1 M_{i-1}^1 \\ \vdots \\ B_i^{2N-1} M_{i-1}^{2N-1} \end{pmatrix}}_{\text{set } i-1} + \underbrace{\begin{pmatrix} C_i^0 M_i^0 \\ C_i^1 M_i^1 \\ \vdots \\ C_i^{2N-1} M_i^{2N-1} \end{pmatrix}}_{\text{set } i} - \underbrace{\begin{pmatrix} D_i^0 M_{i+1}^0 \\ D_i^1 M_{i+1}^1 \\ \vdots \\ D_i^{2N-1} M_{i+1}^{2N-1} \end{pmatrix}}_{\text{set } i+1} \quad (30)$$

244 The three sets of moments in Eq. (30) can easily become non-realizable be-
 245 cause, in general, the coefficients B_i^k as well as C_i^k and D_i^k might differ from
 246 one moment to another (belonging to the same moment set) as a consequence
 247 of unequal limiters. Marchisio and Fox [1] showed that a small change in just
 248 one moment can make a consistent set of moments non-realizable. On the
 249 other hand, if identical limiters are selected to estimate the fluxes of all the
 250 moments at the left and right faces, Eq. (30) can be written as follows:

$$\int_0^\infty f_i^* \mathbf{q}(L) dL = \int_0^\infty (B_i f_{i-1} + C_i f_i - D_i f_{i+1}) \mathbf{q}(L) dL \quad (31)$$

251 OR

$$f_i^* = B_i f_{i-1} + C_i f_i - D_i f_{i+1} \quad (32)$$

252 where B_i as well as C_i and D_i are defined below by choosing an equal limiter
 253 at the left face, $\phi(\theta_{i-1/2})$, and one at the right face, $\phi(\theta_{i+1/2})$, for all the
 254 moments:

$$\begin{aligned} B_i &= \nu - \frac{1}{2}\nu(1-\nu)\phi(\theta_{i-1/2}) \\ C_i &= 1 - \nu + \frac{1}{2}\nu(1-\nu)[\phi(\theta_{i+1/2}) + \phi(\theta_{i-1/2})] \\ D_i &= \frac{1}{2}\nu(1-\nu)\phi(\theta_{i+1/2}) \end{aligned} \quad (33)$$

255 It should be noted that there is still no proof for the moment realizability
 256 in the case of employing equal limiters when source terms in the moment
 257 transport equation are present, because the last term in Eq. (32) is negative
 258 [4] [6]. However, the contribution of the negative term can be kept small
 259 enough through adjusting the time step since the coefficient D_i diminishes as
 260 the time step is reduced to zero. In other words, the non-realizability problem

261 can be prevented by adjusting the time step, whereas it can arise easily
262 regardless of the time step if the limiters are calculated independently. One
263 should be careful when the moment sets lie on the boundary of the moment
264 space. In such case, the underlying number density functions are indeed
265 some point distributions, i.e summation of some weighted delta functions.
266 Therefore, if the moment sets in Eq. (30) are near or on the boundary of the
267 moment space, reduction of the time step cannot resolve the realizability issue
268 since the supports of the corresponding underlying number density functions
269 in Eq. (32) may hardly match each other. A possible remedy can be adopting
270 the 1-D adaptive quadrature technique proposed by Yuan and co-workers [19].
271 By this technique, the maximum number of quadrature nodes is selected in
272 such a way that the moments required to calculate the quadrature weights
273 and abscissas form a set which is located in the interior of the moment space.
274 It is noteworthy that the local reduction of the number of quadrature nodes
275 is not a problem for the equal-limiter scheme, in contrast to the quasi-high-
276 order scheme, since the variables to be interpolated are the moments and not
277 the quadrature abscissas and weights.

278 The final point to be addressed is the choice of an equal flux-limiter at
279 each face. In fact, the constraint on the boundedness of the solution narrows
280 the choice of the equal flux-limiter. As mentioned before, the 2nd-order TVD
281 schemes have this notable feature of preserving the solution bounded. It is
282 extremely useful for the QMOM since the low-order moments are propor-
283 tional to physical properties that are bounded in nature, such as mean size,
284 surface area or volume fraction. Harten [20] established the sufficient crite-
285 ria for a scheme to be TVD, which provide constraints on the flux-limiter

286 functions:

$$\phi(\theta) = 0 \quad \text{if } \theta < 0 \quad \text{and} \quad 0 \leq \phi(\theta) \leq \min(2\theta, 2) \quad \text{if } \theta \geq 0 \quad (34)$$

287 Fig. 1 represents these constraints graphically (shaded area) following the
 288 work of Sweby [21]. Moreover, it depicts the 2nd-order region proposed by
 289 Sweby [21] (hatched area) within which the flux-limiter functions lie. Two
 290 such examples are shown by the solid line (minmod limiter [17]) and the
 291 dashed line (van Leer limiter [18]).

292 The flux-limiter functions in the literature share the common feature of
 293 being non-decreasing functions of θ . Using this feature, it is simple to show
 294 that the smallest flux-limiter among all the limiters of the moments is an
 295 obvious choice that guarantees the boundedness of all the moments. The
 296 flux-limiters calculated independently by a general limiter function at a given
 297 face, e , can be represented as $\phi(\theta_e^k)$ with $k = 0, 1, \dots, 2N - 1$. These limiters
 298 respect the conditions expressed in Eq. (34):

$$\phi(\theta_e^k) = 0 \quad \text{if } \theta_e^k < 0 \quad \text{and} \quad 0 \leq \phi(\theta_e^k) \leq \min(2\theta_e^k, 2) \quad \text{if } \theta_e^k \geq 0 \quad (35)$$

299 Suppose that ϕ_e^{\min} denotes the limiter with the minimum value:

$$\phi_e^{\min} = \phi(\theta_e^m) \leq \phi(\theta_e^k) \quad \text{for } k = 0, 1, \dots, 2N - 1 \quad (36)$$

300 where

$$\theta_e^m \in \{\theta_e^k \mid k \in \{0, 1, \dots, 2N - 1\}\} \quad (37)$$

301 and since the flux-limiter functions are non-decreasing:

$$\theta_e^m \leq \theta_e^k \quad \text{for } k = 0, 1, \dots, 2N - 1 \quad (38)$$

302 On the other hand, the upper boundary of the TVD region shown in Eq. (35),
 303 $\min(2\theta_e^k, 2)$, is a non-decreasing function, therefore:

$$\min(2\theta_e^m, 2) \leq \min(2\theta_e^k, 2) \quad \text{for } k = 0, 1, \dots, 2N - 1 \quad (39)$$

304 since ϕ_e^{\min} respects the conditions specified in Eq. (35), it can be concluded
 305 that:

$$0 \leq \phi_e^{\min} \leq \min(2\theta_e^k, 2) \quad \text{for } k = 0, 1, \dots, 2N - 1 \quad (40)$$

306 in other words, ϕ_e^{\min} falls always in the TVD region specified in Fig. 1 for all
 307 the moments. As a result, the moments remain bounded using this limiter,
 308 following the proof given by Harten [20].

309 It should be mentioned that, in general, the minimum limiter can fall
 310 outside the 2nd-order region of Sweby for some moments, hence resulting in
 311 solutions with accuracy of lower order. Nevertheless, the numerical results
 312 reported in the next section show remarkable improvements in comparison
 313 to the 1st-order solutions. More importantly, the results indicate a significant
 314 advantage of the proposed scheme over the realizable high-order scheme of
 315 Vikas et al. [6] since it is able to produce bounded solutions.

316 4. Application to CFD Codes

317 This section focuses on the application of the equal-limiter scheme to CFD
 318 codes, which is indeed our ultimate goal of introducing this scheme. For this
 319 purpose, the following three-dimensional conservative transport equation is
 320 considered for the k^{th} -order moment:

$$\frac{\partial M^k}{\partial t} + \frac{\partial}{\partial \mathbf{x}} \cdot (\mathbf{u}M^k) = 0 \quad (41)$$

321 The source term is not included since the focus is only on the advection of the
 322 moments. In the context of finite volume methods, Eq. (41) is integrated over
 323 the volume of each computational cell and then the integral of the convective
 324 term over the volume of each cell is replaced with the net flux of the moment
 325 through the faces of that cell (Gauss's theorem). Therefore, the following
 326 semi-discretized equation is obtained for a generic cell i [16]:

$$\frac{dM_i^k}{dt} + \frac{1}{\Delta V_i} \sum_e (\mathbf{u}_e \cdot \hat{\mathbf{n}}_e) S_e M_e^k = 0 \quad (42)$$

327 where M_e^k and \mathbf{u}_e are the moment of order k and the velocity at a generic
 328 face e of cell i respectively. In addition, $\hat{\mathbf{n}}_e$ and S_e denote respectively the
 329 outward unit normal vector and the surface area of face e and ΔV_i is the
 330 volume of the cell i . The transient term in Eq. (42) is not discretized for the
 331 reason that becomes clear later. In CFD codes, the flux of the velocity field
 332 at the cell faces, i.e. $(\mathbf{u}_e \cdot \hat{\mathbf{n}}_e) S_e$, is generally known. However, the value of
 333 the moments at the faces (M_e^k) is not available and should be interpolated
 334 from the values at the centers of neighbouring cells.

335 The implementation of high-resolution TVD schemes in CFD codes is usually
 336 on the basis of central-difference scheme, of which the anti-diffusive contri-
 337 bution is limited to prevent oscillations in the solution [22]:

$$M_e^k = \underbrace{M_U^k}_{\text{upwind}} + \phi(\theta_e^k) \underbrace{\lambda_e (M_D^k - M_U^k)}_{\text{anti-diffusive part}} \quad (43)$$

338 where M_U^k and M_D^k refer to the values of the moment of order k at the centers
 339 of the upwind and downwind cell neighbours of the face e respectively. The
 340 selection of the upwind and downwind cells is based on the direction of the
 341 velocity field at face e , which is the same for all the moments. In addition,

342 the coefficient λ_e takes a positive constant value between 0 and 0.5, which
 343 depends on the distances between the center of face e and the centers of
 344 the two neighbouring cells. The advantage of employing an identical limiter
 345 can be illustrated by rearranging Eq. (43) and writing it for a set of $2N - 1$
 346 moments as follows:

$$\underbrace{\begin{pmatrix} M_e^0 \\ M_e^1 \\ \vdots \\ M_e^{2N-1} \end{pmatrix}}_{\text{set } e} = \underbrace{\begin{pmatrix} [1 - \lambda_e \phi(\theta_e^0)] M_U^0 \\ [1 - \lambda_e \phi(\theta_e^1)] M_U^1 \\ \vdots \\ [1 - \lambda_e \phi(\theta_e^{2N-1})] M_U^{2N-1} \end{pmatrix}}_{\text{set U}} + \underbrace{\begin{pmatrix} \lambda_e \phi(\theta_e^0) M_D^0 \\ \lambda_e \phi(\theta_e^1) M_D^1 \\ \vdots \\ \lambda_e \phi(\theta_e^{2N-1}) M_D^{2N-1} \end{pmatrix}}_{\text{set D}} \quad (44)$$

347 In general, the limiters for different moments, $\phi(\theta_e^0), \phi(\theta_e^1), \dots, \phi(\theta_e^{2N-1})$ are
 348 not the same. Therefore, the moment sets "U" and "D" can easily become
 349 non-realizable, leading to the non-realizable set of interpolated moments at
 350 face e . However, selecting an identical limiter, let it be ϕ_e^{\min} , guarantees the
 351 realizability of the interpolated moment set e , as long as the moment sets
 352 "U" and "D" are realizable:

$$\underbrace{\begin{pmatrix} M_e^0 \\ M_e^1 \\ \vdots \\ M_e^{2N-1} \end{pmatrix}}_{\text{set } e} = (1 - \lambda_e \phi_e^{\min}) \underbrace{\begin{pmatrix} M_U^0 \\ M_U^1 \\ \vdots \\ M_U^{2N-1} \end{pmatrix}}_{\text{set U}} + \lambda_e \phi_e^{\min} \underbrace{\begin{pmatrix} M_D^0 \\ M_D^1 \\ \vdots \\ M_D^{2N-1} \end{pmatrix}}_{\text{set D}} \quad (45)$$

353 It is worth reiterating that the value of limiter ϕ_e^{\min} is between 0 and 2.
 354 Moreover, the moment sets "U" and "D" belong to the previous time step
 355 if an explicit method is used to advance in time, and therefore they are

356 realizable.

357 It should be noted that the realizability of the interpolated moments on the
 358 faces does not ensure the realizability of the calculated moments at the new
 359 time step. To elaborate, let the transient term in Eq. (42) be integrated using
 360 an explicit Euler scheme [16] and then write the fully-discretized equation
 361 for the set of $2N - 1$ moments:

$$\mathbf{W}_i^{n+1} = \mathbf{W}_i^n - \frac{\Delta t}{\Delta V_i} \sum_e (\mathbf{u}_e^n \cdot \hat{\mathbf{n}}_e) S_e \mathbf{W}_e^n \quad (46)$$

362 The use of an identical limiter for all the moments guarantees that the mo-
 363 ment set \mathbf{W}_e^n be realizable, and therefore an underlying number density func-
 364 tion (f_e^n) can be associated to it. This allows writing Eq. (46) as:

$$f_i^{n+1} = f_i^n - \frac{\Delta t}{\Delta V_i} \sum_e (\mathbf{u}_e^n \cdot \hat{\mathbf{n}}_e) S_e f_e^n \quad (47)$$

365 The summation in the above equation can be separated into two contributions
 366 of in-going and out-going fluxes:

$$f_i^{n+1} = f_i^n - \underbrace{\frac{\Delta t}{\Delta V_i} \sum_e \min[(\mathbf{u}_e^n \cdot \hat{\mathbf{n}}_e), 0] S_e f_e^n}_{\text{in-going fluxes}} - \underbrace{\frac{\Delta t}{\Delta V_i} \sum_e \max[(\mathbf{u}_e^n \cdot \hat{\mathbf{n}}_e), 0] S_e f_e^n}_{\text{out-going fluxes}} \quad (48)$$

367 The in-going fluxes have positive sign and cannot rise the realizability issue,
 368 whereas, the outgoing fluxes have negative sign and can cause realizability is-
 369 sue, i.e. negativity of f_i^{n+1} . However, the out-going fluxes can be still decom-
 370 posed into two separate upwind and downwind contributions corresponding
 371 to the upwind and downwind neighbouring cells of the corresponding faces.
 372 It is noteworthy that the upwind cell of these faces indeed coincides with cell

373 i since the flux at these faces is out-going. Thus, the first and third terms of
 374 the RHS of Eq. (48) can be written as follows:

$$\begin{aligned} & \left(1 - (1 - \lambda_e \phi_e^{\min}) \frac{\Delta t}{\Delta V_i} \sum_e \max[(\mathbf{u}_e^n \cdot \hat{\mathbf{n}}_e), 0] S_e \right) f_i^n \\ & - (1 - \lambda_e \phi_e^{\min}) \frac{\Delta t}{\Delta V_i} \sum_e \max[(\mathbf{u}_e^n \cdot \hat{\mathbf{n}}_e), 0] S_e f_{D_e}^n \end{aligned} \quad (49)$$

375 where $f_{D_e}^n$ denotes the (downwind) neighbouring cell separated by face e from
 376 cell i . As can be seen, the entire contribution of the cell i is positive as long
 377 as the coefficient behind f_i^n is positive, leading to the following CFL-like
 378 condition:

$$\frac{\Delta t}{\Delta V_i} \sum_e \max[(\mathbf{u}_e^n \cdot \hat{\mathbf{n}}_e), 0] S_e < 1 \quad (50)$$

379 Therefore, the only remaining negative contributions are due to the infor-
 380 mation (distributions) of the downwind cells (with respect to cell i) that
 381 propagates back into cell i , which is the characteristic of high-order schemes.
 382 These negative contributions can generally lead to the non-realizability issue,
 383 i.e. negativity of f_i^{n+1} . However, similar to the previous discussion done for
 384 one-dimensional constant-velocity cases, the negative contributions can be
 385 kept small (in comparison to the contribution of f_i^n) by controlling the time
 386 step. It is noteworthy that this technique may fail as the moment sets are
 387 near/at the boundary of the moment space, as explained before.

388 Returning back to the time-integration of the transient term in Eq. (42),
 389 it should be noted that one notable advantage of the equal-limiter scheme
 390 is the possibility of using implicit time-integration for the advection of the
 391 moments. This is due the fact that the equal-limiter scheme interpolates
 392 the moments directly, whereas, for instance, the quasi-high-order scheme is

393 normally implemented using explicit time-integration schemes. This aspect
394 is particularly important when the solution of the population balance equa-
395 tion is incorporated into a CFD solver, since the implicit time-integration
396 schemes are commonly adopted in these codes.

397 Lastly, the proposed technique is very simple from the computational
398 point of view and can be easily implemented in three-dimensional CFD
399 solvers. The only additional steps are comparing the limiter values calculated
400 for the moments at each face and then replacing them with the smallest one
401 at the corresponding face.

402 **5. Numerical Examples**

403 This section evaluates the performance of the proposed technique for the
404 advection of moments in two different parts. The first one is focused on com-
405 paring the predictions obtained by different schemes for the advection of the
406 moments in a mono-dimensional constant-velocity problem. The second part
407 evaluates the performance of the schemes by solving the moment transport
408 equations coupled with the CFD simulation of a two-dimensional transient
409 lid-driven cavity flow.

410 *5.1. One-dimensional advection with constant-velocity*

411 This part employs the equal-limiter scheme for the advection of moments
412 in spatially mono-dimensional problems with the disperse particle size as the
413 only internal coordinate of the PBE. The first example deals with the pure
414 advection of the moments without any source term, while the next examples
415 includes the aggregation/breakage source terms in the moment transport
416 equations. The results are compared with those obtained via a 1st-order

417 scheme and the realizable high-order scheme (or quasi-2nd-order scheme) by
418 Vikas et al. [6]. In addition, the analytical solution is reported whenever it
419 is available.

420 All the cases use 3-node quadrature to approximate the NDF. This num-
421 ber of nodes requires to track the first 6 moments with respect to the par-
422 ticle size, M^0, M^1, \dots, M^5 . The calculation of the weights and abscissas of
423 the quadrature is done by using the Chebyshev algorithm. The spatial prob-
424 lems are defined over the spatial domain $[0, 1]$, which is discretized to cells
425 of identical size $\Delta x = 0.01$. The fluxes at the faces are calculated using
426 high-resolution limited-flux methods. The limiters, in turn, are computed
427 using the minmod function, as it was also used by Vikas et al [6]. Two ghost
428 cells at the left side of the domain and one ghost cell at the right side are
429 considered to cope with the three-cell stencil required by the high-resolution
430 schemes. The advection velocity, u , is set to 1.0 and Δt is calculated by
431 fixing the CFL condition equal to 0.5. The following solution procedure is
432 used to advance in time starting from the initial data, which is based on the
433 explicit fractional-step method for time integration:

- 434 1. Initialize the moments in the interior domain.
- 435 2. Apply the boundary conditions at the two left ghost cells.
- 436 3. Calculate the limiters for all the moments at each face.
- 437 4. Find the minimum limiter at each face.
- 438 5. Calculate the flux of the moments using the minimum limiter at each
439 face.

- 440 6. Compute the intermediate values of the moments at each interior cell
441 using the fluxes at the corresponding left and right faces after a time
442 step equal to Δt .
- 443 7. Find the weights and the abscissas of the quadrature at each interior
444 cell using the intermediate values of the moments.
- 445 8. Calculate the source contributions at each interior cell using the corre-
446 sponding quadrature approximation of the NDF.
- 447 9. Advance the intermediate values of the moments at each interior cell
448 by one time step Δt using the calculated source terms.
- 449 10. Apply the boundary condition at the right ghost cell using zero-order
450 extrapolation from the last interior cell of the domain.
- 451 11. Repeat steps 3 to 10 until obtaining the solution at the desired time.

452 Steps 8 and 9 (fractional-step approach) are obviously required only if the
453 source terms are present. In this work, the source terms are treated by a
454 single-stage method as explained in steps 8 and 9. However, these steps can
455 be modified to use a two-stage method, leading to higher accuracy for the
456 fractional-step approach as explained by LeVeque [15]. It should be empha-
457 sized that this suggestion concerns the application of two-stage methods only
458 for updating the intermediate moments by the source terms. Therefore, no
459 realizability issue is generally expected in case of using two-stage methods
460 instead of one-stage method only to treat the source terms, provided that
461 the intermediate moments after the advection are realizable. Furthermore,

462 step 7 is done even in the case without source term to check the realizability
 463 of the moments.

464 More details on the problem settings are presented for each case sepa-
 465 rately.

466 *5.1.1. Pure advection of the moments*

467 The first example is the one-dimensional pure advection of the moments,
 468 i.e. no source term, with the following initial and boundary conditions:

$$\begin{aligned}
 IC : \quad M^k(x_i, 0) &= \overset{\circ}{M}^k \quad \text{for } i = 0, 1, 2, \dots, p \\
 BC \text{ (ghost cells)} : \quad &\begin{cases} M^k(x_{-1}, t_n) = M^k(x_{-2}, t_n) = M_b^k \\ M^k(x_{p+1}, t_n) = M^k(x_p, t_n) \end{cases} \quad (51)
 \end{aligned}$$

469 where the interior cells are numbered from 0 to p . The initial conditions
 470 $\overset{\circ}{M}^k$ and the boundary conditions M_b^k are two sets of scaled moments having
 471 the shape of different log-normal distributions, $\overset{\circ}{Y}$ and Y_b . The parameters
 472 of the distributions, i.e. the mean and the standard deviation of the cor-
 473 responding normal distributions, are respectively $(\overset{\circ}{\mu}, \overset{\circ}{\sigma}) = (\ln(0.008), 0.22)$
 474 and $(\mu_b, \sigma_b) = (\ln(0.005), 0.2)$. Furthermore, the zero-order moments are
 475 $\overset{\circ}{M}^0 = 20000$ and $M_b^0 = 800000$ respectively. It should be noted that the two
 476 log-normal distributions have different parameters to avoid their quadra-
 477 ture approximations having the same abscissas. Otherwise, the interpolated
 478 abscissas on the faces are identical to those of the cells regardless of the
 479 employed scheme. Then, it is trivial to show that, in this special case, the
 480 quasi-2nd-order scheme proposed by Vikas et al. [6] is essentially the same
 481 as applying 2nd-order scheme directly to the moments.

482 Figure 2 compares the results obtained from 1st-order scheme, quasi-2nd-

483 order scheme and the proposed equal-limiter scheme. Furthermore, the an-
484 analytical solution is plotted in Fig. 2 to provide a benchmark. It is pointless
485 to report the results by the standard 2nd-order TVD scheme since, as proved
486 before, the corresponding results would be identical to those obtained by
487 the equal-limiter scheme. As expected, the solution given by the 1st-order
488 scheme is very diffusive. The quasi-2nd-order scheme improves the accuracy
489 of the results by applying 2nd-order scheme to the weights. However, the
490 moments do not remain bounded simply because applying a TVD scheme
491 to the weights does not guarantee the boundedness of the transported mo-
492 ments, hence appearance of the non-physical oscillations in the solutions.
493 The least oscillations belong to the moment of order zero as expected, since
494 it is simply equivalent to the sum of the weights, the variable to which the
495 TVD scheme is applied in the quasi-2nd-order scheme. The oscillations be-
496 come more obvious as the moment order increases. It should be noted that,
497 according to our tests, the oscillations may increase or vanish depending on
498 the characteristics of the underlying NDFs. The best predictions belong to
499 the equal-limiter scheme which is indeed the full 2nd-order TVD scheme since
500 this numerical example is the same as the pure advection Riemann problem
501 studied in Section 3. Consequently, the predictions are bounded and without
502 any oscillation.

503 *5.1.2. Moment advection with source term*

504 The next examples deal with a more practical application. The moments
505 of a particle size distribution are introduced and advected in the domain while
506 they are subject to local changes due the effect of the aggregation/breakage
507 of the particles. The initial and boundary conditions are the same as the case

508 of pure advection (see Eq. (51)). In the following, two cases are presented
 509 in which the aggregation and breakage are considered separately. Both ag-
 510 gregation and breakage are modeled by assuming a constant kernel. For the
 511 case of breakage, the daughter size distribution is expressed by assuming
 512 symmetric fragmentation of the particles [23]. The reasoning behind these
 513 simplistic assumptions is the possibility of obtaining analytical solutions for
 514 the moments of the NDF.

515 **Constant aggregation kernel.** In this case, the source term in Eq. (7) is
 516 calculated as follows [23]:

$$h_i^k = \frac{1}{2} \sum_{\alpha=1}^3 w_{i,\alpha} \sum_{\beta=1}^3 w_{i,\beta} (L_{i,\alpha}^3 + L_{i,\beta}^3)^{k/3} K_a - \sum_{\alpha=1}^3 L_{i,\alpha}^k w_{i,\alpha} \sum_{\beta=1}^3 w_{i,\beta} K_a \quad (52)$$

517 where $K_a = 10^{-5} (m^3 \cdot s^{-1})$ is the aggregation kernel.

518 The solutions obtained by the studied schemes are shown in Fig. 3. As can
 519 be seen, both quasi-2nd-order and equal-limiter schemes improve the accuracy
 520 of the results with respect to the 1st-order scheme. It is notable that, despite
 521 employing the minimum limiter, the equal-limiter scheme produces almost
 522 comparable results to those of the quasi-2nd-order scheme. Moreover, the
 523 solutions of M^3 indicate that only 1st-order and equal-limiter schemes are
 524 bounded, as expected. Instead, a slight degree of overshoot and undershoot
 525 exists in the solution of the quasi-2nd-order scheme. The appearance of these
 526 spurious oscillations is certainly due to the numerics as both aggregation and
 527 breakage of the particles have no effect on the moment of order three with
 528 respect to the particle size. Although no analytical solution is available for
 529 M^5 , some degree of overshoot and undershoot can be observed visually in
 530 the solution obtained by the quasi-2nd-order scheme. Again it can be seen

531 that the amplitude of the oscillations are intensified as the moment order
532 increases. It is worth mentioning that employing the standard 2nd-order
533 TVD scheme is not feasible because the moments get corrupted shortly after
534 starting the simulation and consequently the Chebyshev algorithm fails to
535 calculate the weights and the abscissas required for the source calculation.
536 Even reducing the time step by a factor of 100, equivalent to an impractically
537 small CFL value of 0.005, cannot remedy the non-realizability problem. This
538 shows the effectiveness of the proposed equal-limiter scheme in preserving the
539 realizability of the moments when the 2nd-order TVD schemes are employed.
540 **Symmetric constant breakage kernel.** In this case, the source term in
541 Eq. (7) is calculated as follows [23]:

$$h_i^k = \sum_{\alpha=1}^3 w_{i,\alpha} 2^{(3-k)/3} L_{i,\alpha}^k K_b - \sum_{\alpha=1}^3 w_{i,\alpha} L_{i,\alpha}^k K_b \quad (53)$$

542 where $K_b = 4$ (s^{-1}) is the breakage kernel.

543 Fig. 4 depicts the results provided by the studied schemes along with the
544 analytical solutions. The same arguments presented for the case of pure ag-
545 gregation apply also to this case with the difference that here the oscillating
546 behavior of the quasi 2nd-order scheme is more intense. This further high-
547 lights the advantage of the equal-limiter scheme whenever the boundedness
548 of the solution is strictly required.

549 5.2. *Pure advection in two-dimensional transient flow*

550 The previous part presents satisfactory results obtained by the equal-
551 limiter scheme in the one-dimensional constant-velocity Riemann problem
552 examples. However, it is important to examine the predictions obtainable
553 by the proposed scheme in systems with higher dimensions and realistic flow

554 fields, e.g. non-constant and/or transient velocity. For this purpose, a famil-
555 iar two-dimensional transient flow, known as lid-driven cavity, is selected to
556 compare the results for the pure advection of moments obtained by employ-
557 ing upwind, quasi-2nd-order and equal-limiter schemes. The moments belong
558 to the distributions that represent the population of micro-droplets which
559 are transported by a carrier liquid. The micro-droplets are assumed to do
560 not have their own inertia and therefore they move with the same velocity
561 of the carrier liquid.

562 The simulation domain is a square with length (L) of 10 cm and it is dis-
563 cretized by a structured uniform Cartesian grid comprising of 10000 square
564 cells of size 1 mm. The flow is confined by four boundaries of type wall, from
565 which the top one moves with the velocity (U) of 1 (m/s) while the others are
566 fixed. The kinematic viscosity of the liquid (ν) is set to 2.5×10^{-4} (m²/s),
567 which results to Reynolds number of 400 defined by UL/ν . The liquid is
568 assumed to be stagnant at time zero and then a transient flow develops in
569 the liquid due to the constant velocity (U) applied at the top wall.

570 The transient simulations are done by using the icoFoam solver of Open-
571 FOAM software, which solves the governing (constant-density) Navier-Stokes
572 equations for the liquid phase numerically by using the PISO algorithm [16].
573 The time step is set to 0.0001 (s) to keep the maximum Courant number
574 below 0.1. The solution of the velocity field at three time instants are shown
575 in Fig. 5. The solver is modified to solve simultaneously the moment trans-
576 port equations. At the beginning of each time step, the moments of the
577 micro-droplet population are advected in time using the velocity field of the
578 previous time step. Then, the flow field of the liquid phase is updated by us-

579 ing the PISO algorithm. Regarding the advection of moments, as mentioned
580 in Section 4, the implicit Euler time-integration can be used with the advec-
581 tion schemes that deal with the moments directly, and therefore is adopted
582 here when the upwind and equal-limiter schemes are employed. On the other
583 hand, the quasi-2nd-order scheme is implemented with Euler explicit time-
584 integration. It should be noted that the reasoning behind employing the
585 implicit time-integration scheme is to highlight the advantage of the equal-
586 limiter scheme, which is its compatibility with the implicit approach. Con-
587 cerning the flux-limiter, the minmod function is used for the interpolation
588 of quadrature weights in case of employing quasi-2nd-order scheme and the
589 interpolation of moments in case of employing equal-limiter scheme.

590 Two different cases corresponding to two different initial conditions for the
591 moments are considered. The first initial condition is defined such that there
592 is no micro-droplets in the domain except for a square patch where a popu-
593 lation of micro droplets with average size of 100 (μm) and standard devia-
594 tion of 20 (μm) is introduced. The population is assumed to be distributed
595 log-normally on the size space. The initial conditions for the moments are
596 calculated based on this log-normal distribution which is scaled to adjust the
597 volume fraction of the micro-droplets equal to 0.05 (assuming spherical shape
598 for the micro-droplets). Fig. 6 depicts the initial conditions for the moment
599 of order three, along with the solutions for the same moment at $t = 3$ s ob-
600 tained by employing the 1st-order upwind, quasi-2nd-order and equal-limiter
601 schemes. As can be seen, the solution obtained by the upwind scheme suffers
602 from high numerical diffusion. On the other hand, both the quasi-2nd-order
603 and equal-limiter schemes yield comparable results, which have higher resolu-

604 tion with respect to the one obtained by the upwind scheme. It is noteworthy
605 that the same contour plots (but of different values) are obtained for the other
606 moments, which is expected since the shape of the distribution corresponding
607 to the underlying NDF remains the same in pure advection. As a result, the
608 abscissas of the quadrature approximation are the same in all the cells of the
609 domain.

610 As mentioned previously, the quasi-2nd-order scheme interpolates the quadra-
611 ture abscissas with a 1st-order scheme, whereas it interpolates the quadrature
612 weights with a 2nd-order scheme. Therefore, when the quadrature abscissas
613 are the same throughout the domain, the entire resolution of the quasi-2nd-
614 order scheme for the pure advection of moments is the same as the 2nd-order
615 scheme. The reason is that, in this case, the value of abscissas on the faces are
616 the same as those at the cell centers regardless of the employed scheme. Con-
617 sequently, the pure advection of moments by interpolating the weights onto
618 the faces with a given 2nd-order scheme and then constructing the moments
619 on the faces (using the same abscissas) is equivalent to the pure advection
620 of moments by interpolating the moments directly onto the faces using that
621 2nd-order scheme. However, this equivalency is not generally valid when the
622 abscissas are not the same through the domain. Thus, it is worth examining
623 the performance of the schemes in case of existing two different distributions,
624 i.e. having different quadrature abscissas, in the system at time zero. For
625 this purpose, the same square patch (with the same population of micro-
626 droplets) defined by the initial conditions of the previous case is considered
627 also here. However, it is assumed that another population of micro-droplet
628 exists outside the square patch, instead of assuming no micro-droplet existing

629 in that zone. Let the population of micro-droplets out of the square patch
630 be also distributed log-normally on the size space with average size equal to
631 $50 \text{ } (\mu\text{m})$ and standard deviation of $7.5 \text{ } (\mu\text{m})$. This distribution is scaled to
632 have the volume fraction of the micro-droplets equal to 0.001. Then, the ini-
633 tial condition of the moments is defined based on this scaled distribution, as
634 shown in Figs. 7 and 8 for the moments of order zero and three respectively.
635 Moreover, the predictions at $t = 3 \text{ s}$ are depicted by these figures for the
636 mentioned moments. As can be seen in Fig. 7, the values of M_0 obtained by
637 employing the quasi-2nd-order scheme do not remain bounded between the
638 limits defined by the initial conditions. It is noteworthy that in QBMM, the
639 transported variables are indeed the moments and therefore in the pure ad-
640 vection with a solenoidal velocity field, the solution for the moments should
641 remain bounded between the limits defined by the initial conditions. This
642 issue concerning the quasi-2nd-order scheme can be associated to the fact
643 that this scheme interpolates the weights and abscissas of the quadrature
644 separately, and therefore there is no guarantee that the TVD criteria [20] are
645 respected by this scheme. On the other hand, the solution obtained by the
646 equal-limiter scheme (when it is used with the minimum limiter) respects
647 the boundedness property of the moments. Moreover, the applied change in
648 the initial condition of the moments should not change the pattern of the
649 solution contour plots, since the current initial condition with the two dis-
650 tributions can be changed to a problem with initial condition similar to the
651 previous case (micro droplets existing only in a square patches) by a change
652 of variables. However, the comparison between the results shown in Fig. 8
653 with those depicted in Fig. 6 highlights that only the equal-limiter scheme

654 reproduces the same pattern for M_3 in both cases. Furthermore, the pattern
655 of the results obtained by the equal-limiter scheme for M_0 and M_3 shown
656 in Figs. 7 and 8 are the same, whereas this is not the case for the results
657 obtained by the quasi-2nd-order scheme. This final example emphasizes the
658 advantage of employing a scheme which interpolates the moments directly,
659 e.g. equal-limiter scheme, instead of interpolating some variables related to
660 the moments.

661 **6. Conclusions**

662 A new technique called equal-limiter scheme was proposed to overcome
663 the non-realizability problem that arises when the 2nd-order TVD schemes
664 are employed to solve the moment transport equations in the context of
665 QBMM. The central idea behind the technique is that the interpolated mo-
666 ments on the faces must form a realizable set when the moment fluxes are
667 being calculated. Following this idea, it was explained that using an identical
668 flux-limiter for all the moments at each face guarantees the realizability of
669 the interpolated moments and consequently helps to preserve the realizabil-
670 ity of the transported moments. Although no formal proof has been given
671 to ensure that the equal-limiter scheme preserves the realizability of the mo-
672 ments under general conditions, it has been shown that this feature can be
673 achieved in the limit of small time steps (as long as the moment sets are
674 far from the boundary of the moment space). On the contrary, adjusting
675 the time step can not mitigate the non-realizability problem if the limiters
676 are independently calculated for each moment of the transported moment
677 set. This fact was also illustrated by the numerical tests as the moments

678 did not remain realizable even with impractically small time step in the case
679 of employing the standard 2nd-order TVD scheme. Moreover, it was proved
680 that the minimum limiter is a possible practical option for the equal limiter
681 if the boundedness feature of the TVD schemes has to be retained. Al-
682 though selecting the minimum limiter may imply solutions of lower order,
683 the one-dimensional numerical examples showed that the results obtained by
684 equal-limiter and quasi-2nd-order schemes are comparable in terms of accu-
685 racy. More importantly, the improvement in the accuracy was observed also
686 for the solutions obtained by the equal-limiter scheme in a one-way coupled
687 QMOM-CFD simulation of a transient two-dimensional flow. Furthermore,
688 the new technique does not only improve the accuracy of the solution with
689 respect to the 1st-order solution but also keeps the solution bounded, which
690 was shown to be an advantage over the quasi-2nd-order scheme by comparing
691 their predictions in both one- and two-dimensional numerical examples. In
692 addition, the implementation of the scheme is simple and can be integrated
693 into the CFD simulations easily.

694 The future works will focus on applying the proposed scheme to the
695 three-dimensional CFD simulation of polydisperse systems and studying its
696 predictions in comparison to those of the other discretization schemes.

697 **References**

- 698 [1] D. L. Marchisio, R. O. Fox, Computational Models for Polydisperse
699 Particulate and Multiphase Systems, Cambridge Series in Chemical En-
700 gineering, Cambridge University Press, Cambridge, UK, 2013.
- 701 [2] R. G. Gordon, Error bounds in equilibrium statistical mechanics, Jour-
702 nal of Mathematical Physics 9 (1968) 655–663.
- 703 [3] J. C. Wheeler, Modified moments and Gaussian quadratures, Rocky
704 Mountain Journal of Mathematics 4 (1974) 287–296.
- 705 [4] O. Desjardins, R. O. Fox, P. Villedieu, A quadrature-based moment
706 method for dilute fluid-particle flows, Journal of Computational Physics
707 227 (2008) 2514–2539.
- 708 [5] D. L. Wright Jr., Numerical advection of moments of the particle size
709 distribution in Eulerian models, Journal of Aerosol Science 38 (2007)
710 352–369.
- 711 [6] V. Vikas, Z. J. Wang, A. Passalacqua, R. O. Fox, Realizable high-order
712 finite-volume schemes for quadrature-based moment methods, Journal
713 of Computational Physics 230 (2011) 5328–5352.
- 714 [7] A. Buffo, M. Vanni, D. L. Marchisio, On the implementation of mo-
715 ment transport equations in openfoam: boundedness and realizability,
716 International Journal of Multiphase Flow 85 (2016) 223–235.
- 717 [8] D. Kah, F. Laurent, M. Massot, S. Jay, A high order moment method

- 718 simulating evaporation and advection of a polydisperse liquid spray,
719 Journal of Computational Physics 231 (2) (2012) 394–422.
- 720 [9] F. Laurent, T. T. Nguyen, Realizable second-order finite-volume
721 schemes for the advection of moment sets of the particle size distri-
722 bution, Journal of Computational Physics 337 (2017) 309–338.
- 723 [10] C. Berthon, et al., Stability of the MUSCL schemes for the Euler equa-
724 tions, Communications in Mathematical Sciences 3 (2) (2005) 133–157.
- 725 [11] D. Ramkrishna, Population Balances: Theory and Applications to Par-
726 ticulate Systems in Engineering, 1st Edition, Academic Press, 2000.
- 727 [12] D. L. Marchisio, R. O. Fox, Solution of population balance equations
728 using the direct quadrature method of moments, Journal of Aerosol
729 Science 36 (2005) 43–73.
- 730 [13] J. A. Shohat, J. D. Tamarkin, The problem of moments, American
731 Mathematical Society, New York, USA, 1943.
- 732 [14] M. Pigou, J. Morchain, P. Fede, M.-I. Penet, G. Laronze, New develop-
733 ments of the extended quadrature method of moments to solve popu-
734 lation balance equations, Journal of Computational Physics 365 (2018)
735 243–268.
- 736 [15] R. J. LeVeque, Finite Volume Methods for Hyperbolic Problems, 1st
737 Edition, Cambridge University Press, 2002.
- 738 [16] J. H. Ferziger, M. Peric, Computational Methods for Fluid Dynamics,
739 3rd Edition, Springer, Berlin, Germany, 2001.

- 740 [17] P. Roe, M. Baines, Algorithms for advection and shock problems, in:
741 Numerical Methods in Fluid Mechanics, 1982, pp. 281–290.
- 742 [18] B. Van Leer, Towards the ultimate conservative difference scheme. II.
743 monotonicity and conservation combined in a second-order scheme,
744 Journal of computational physics 14 (4) (1974) 361–370.
- 745 [19] C. Yuan, R. O. Fox, Conditional quadrature method of moments for
746 kinetic equations, Journal of Computational Physics 230 (2011) 8216–
747 8246.
- 748 [20] A. Harten, High resolution schemes for hyperbolic conservation laws,
749 Journal of computational physics 49 (3) (1983) 357–393.
- 750 [21] P. K. Sweby, High resolution schemes using flux limiters for hyperbolic
751 conservation laws, SIAM journal on numerical analysis 21 (5) (1984)
752 995–1011.
- 753 [22] H. K. Versteeg, W. Malalasekera, An Introduction to Computational
754 Fluid Dynamics: The Finite Volume Method, 2nd Edition, Pearson Ed-
755 ucation, 2007.
- 756 [23] D. L. Marchisio, R. D. Vigil, R. O. Fox, Quadrature method of moments
757 for aggregation-breakage processes, Journal of Colloid and Interface Sci-
758 ence 258 (2003) 322–334.

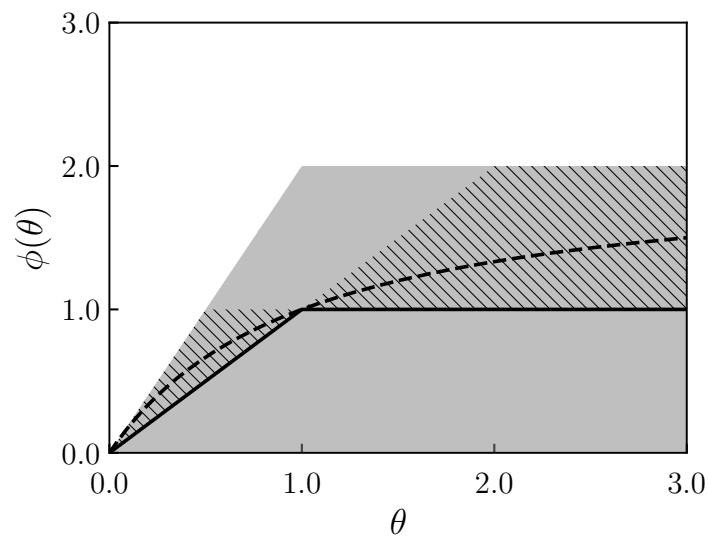


Figure 1: Flux-limiter functions. The shaded area specifies the TVD region and the hatched area is the 2nd-order region by Sweby [21]. The minmod [17] and van Leer [18] limiter functions are shown by the continuous and dashed curves respectively.

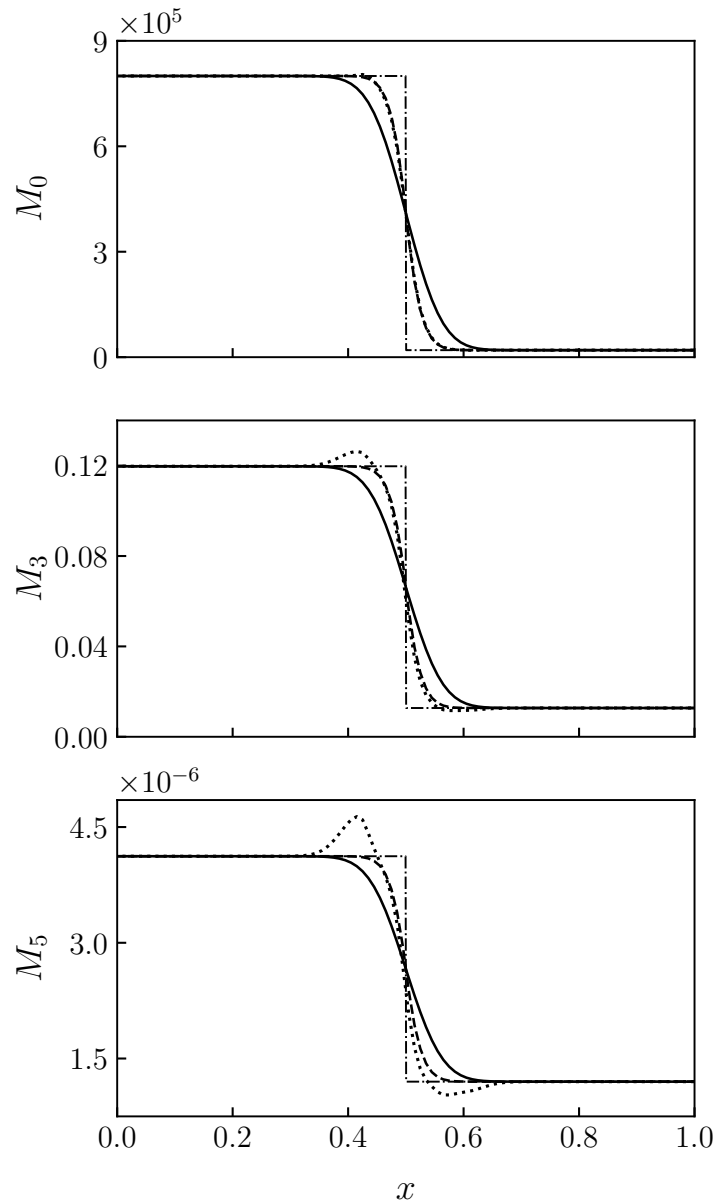


Figure 2: Comparison of the results obtained by employing different schemes for the case of pure advection: 1) analytical solution (dot-dashed line); 2) upwind scheme (continuous line); 3) quasi 2nd-order scheme (dotted line); 4) equal-limiter scheme (dashed line)

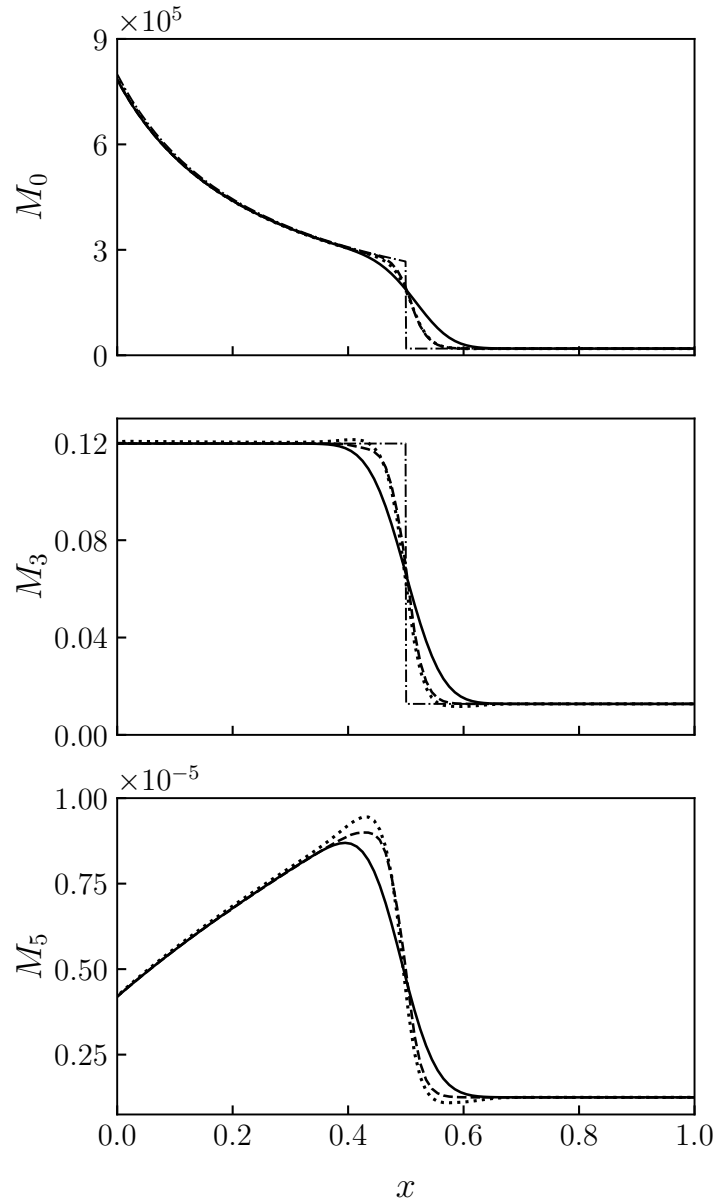


Figure 3: Comparison of the results obtained by employing different schemes for the case of constant aggregation kernel: 1) analytical solution if available (dot-dashed line); 2) upwind scheme (continuous line); 3) quasi 2nd-order scheme (dotted line); 4) equal-limiter scheme (dashed line)

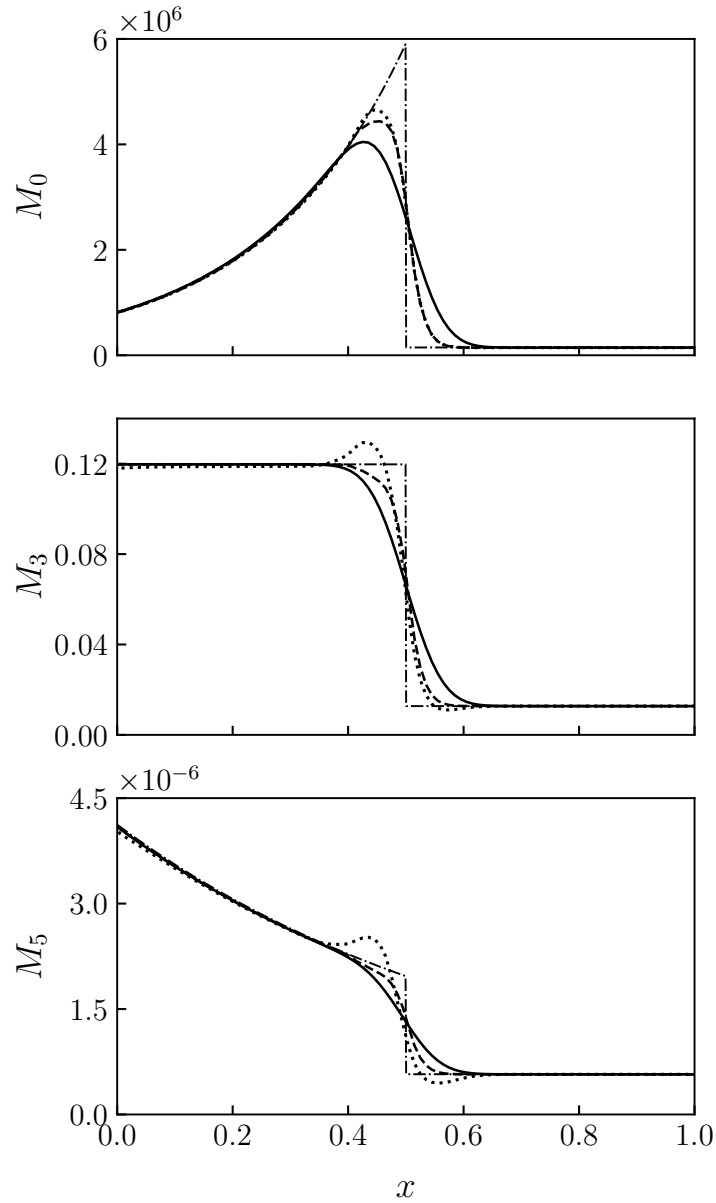


Figure 4: Comparison of the results obtained by employing different schemes for the case of symmetric constant breakage kernel: 1) analytical solution (dot-dashed line); 2) upwind scheme (continuous line); 3) quasi 2nd-order scheme (dotted line); 4) equal-limiter scheme (dashed line)

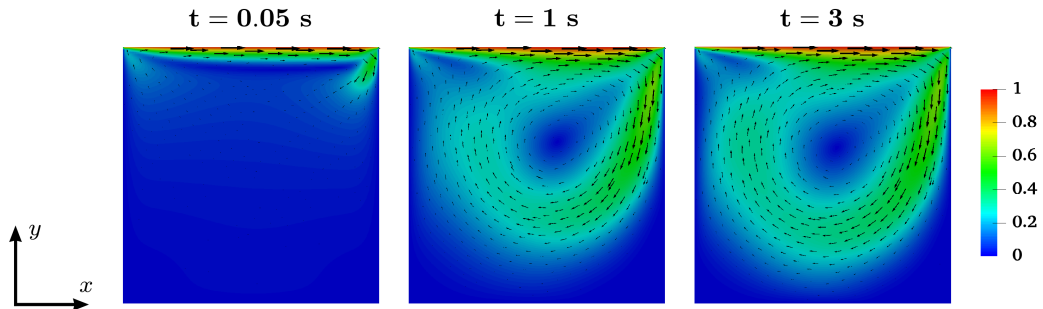


Figure 5: Velocity field (m/s) of the simulated 2-D lid-driven cavity flow at three time instants.

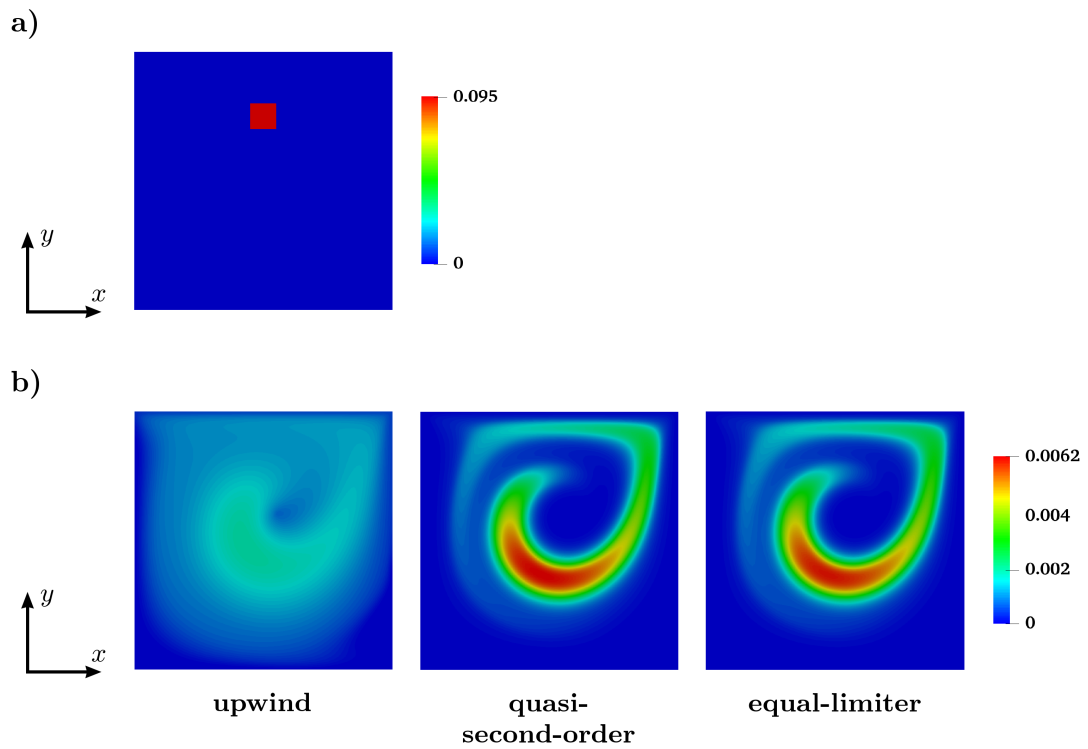


Figure 6: Comparison of the studied schemes for the advection of M_3 in the 2-D cavity flow. (a) The initial condition at $t = 0$; (b) the predictions obtained by employing the different schemes at $t = 3$.

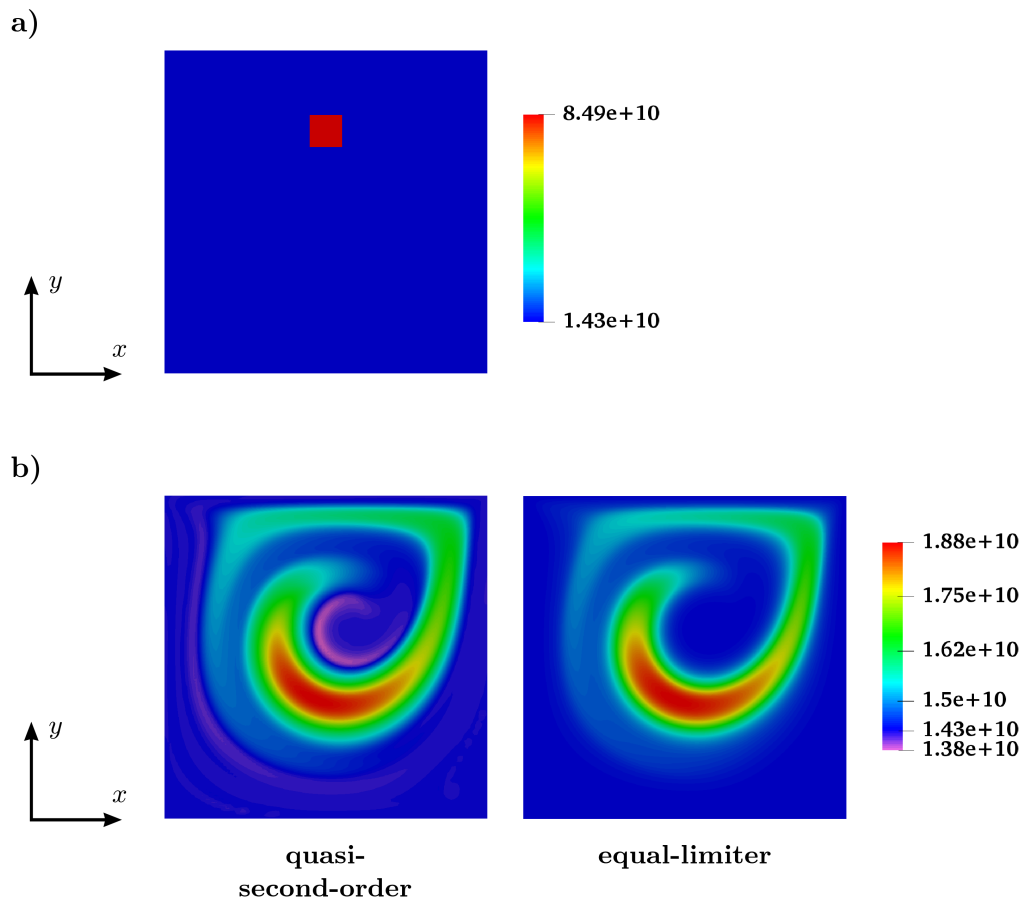


Figure 7: Comparison of the studied schemes for the advection of M_0 in the 2-D cavity flow in case of existing two different distributions in the domain. (a) The initial condition at $t = 0$; (b) the predictions obtained by employing the different schemes at $t = 3$.

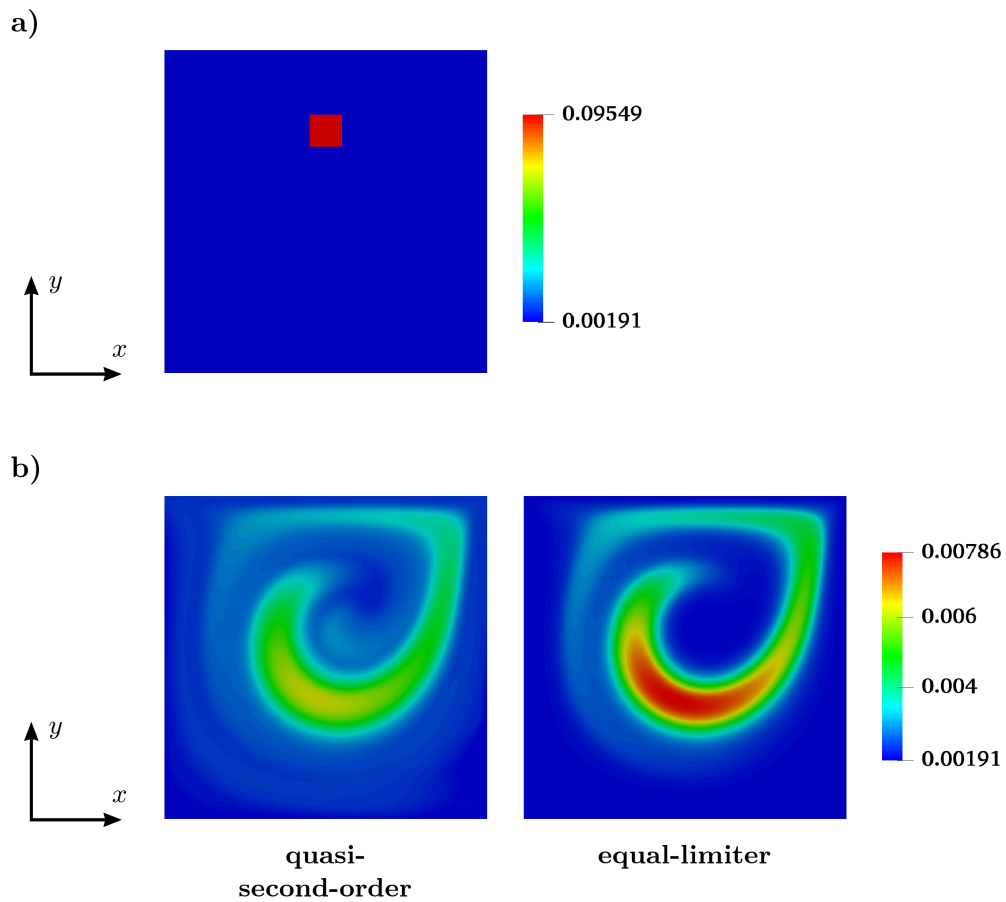


Figure 8: comparison of the studied schemes for the advection of M_3 in the 2-D cavity flow in case of existing two different distributions in the domain. (a) The initial condition at $t = 0$; (b) the predictions obtained by employing the different schemes at $t = 3$.